Laser-based remote detection of leaf wetness

R. Gaetani, François Feugier, Bruno Masenelli

Laser-based Remote Detection of Leaf Wetness

R. Gaetani,[1,2] F.G. Feugier,[1] and B. Masenelli[2]
[1)]*Greenshield, 75004 Paris.*
[2)]*Univ. Lyon, Ecole Centrale de Lyon, INSA Lyon, UCB Lyon, CPE Lyon, CNRS, Lyon Institute of Nanotechnology, UMR5270, Ecully, 69130, France.*

(*Electronic mail: bruno.masenelli@insa-lyon.fr)

(Dated: 11 May 2023)

Pesticide-free agricultural strategies need new tools for diseases prevention. Better than early detection of disease, detection of conditions favorable to their appearance can be a progress. In the case of fungal diseases, the presence of water on the plant surface is necessary. In order to detect remotely this presence early and at the scale of a crop field, we propose a low-cost solution based on laser reflection. Here, experimental results in a controlled environment are presented on both hydrophobic and hydrophilic leaves (respectively rapeseed *Brassica Napus* and grapevine *Vitis Vinifera*). We first assess the water detection on leaf surface by recreating the dew formation process. We next evaluate the influence of the scanning measurement and leaves inclination on the detection to get closer to in-field conditions. Results show that this method is very sensitive on both types of leaves. Water detection is possible from a low surface coverage with a high temporal precision at 1 m. In the hydrophobic case, water on leaf surface leads to an increase of the detected signal up to three times compared to a dry leaf. The corresponding minimum surface coverage detectable at 1 m is evaluated at 1.6% thanks to 2D ray-tracing numerical simulations. In the hydrophilic case, on the contrary, water on leaf surface leads to a decrease of the detected signal by almost half. For both types, the dew detection delay is contained under five minutes and can be improved. Finally, the presented results pave the way to a field application.

I. INTRODUCTION

In agriculture, fungal diseases cause losses both in quantity and quality. They are annually accountable for the destruction of one third of the food production[1]. The impact of crop diseases is widespread, affecting even the most commonly cultivated species such as wheat (*Triticum æstivum*)[2,3]. One example is the spread of septoria, which is caused by the fungus *Zymoseptoria tritici* and can lead to severe epidemics resulting in yield losses of up to 50%[4]. In vineyards, diseases like mildew or grey rot diminish yield by one fourth[5]. They also reduce the production of desirable aroma compounds while inducing undesirable aroma compounds and taste such as pronounced viscous mouthfeel character[5,6]. Fungal diseases proliferate on both hydrophilic and hydrophobic leaves such as respectively grapevine (*Vitis vinifera*) and rapeseed (*Brassica napus*) leaves[7]. In this case, fungal infections lead to a decreased oil yield (up to 30%) but have less influence on oil quality[8,9]. On a more general context, this issue is described as underestimated[10]. A common response is the use of fungicides. This solution is more and more reassessed with the evidence accumulation of health issues[11–13], environmental issues[14,15] and even efficiency issues[16,17]. Hence, reduction strategies are needed. Methods for detecting directly diseases on leaves already exist[18,19] but at this stage, infection has already occurred, which might be considered as too late. Therefore, early plant disease detection is promising for reducing pesticide utilization[20,21]. Going further, the early detection of the necessary conditions for disease development is even better. Cryptogamic diseases usually need water to contaminate. Thus, a tool for wetness monitoring can help farmers to get ahead of diseases and avoid their propagation when events like dew or rain happen. Moreover, knowing the length of the wet period is crucial to evaluate contamination risk. Despite the availability of sensors that measure wetness through changes in resistivity or relative permittivity, they only offer punctual measurements[22,23]. Though, it should be noted that these sensors must be placed in the foliage and their measurement area is limited to that of a single leaf. As a result, they may not provide a representative view of what is happening across a field unless a large number of sensors are purchased. Others are based on computer vision[24] or on differential spectroscopy in the infrared allowing the discrimination between internal and external water. Nonetheless, it is not always possible to achieve this discrimination[25]. Alternatively, as for geometrical sensing based on LIDAR (LIght Detection And Ranging), a laser-based device could allow fast and low-cost remote measurements thanks to its intense and collimated beam. Nicolayev *et al.*[26] developed the idea that dew can be measured by its diffraction pattern using a laser source. In this way, surface coverage and average droplet radius can be retrieved. However, their approach requires a transparent substrate for the deposited drops and is therefore not suitable for a field application. Different laser-based techniques are already applied in remote sensing, such as light depolarization by water droplet[27] or interferometric speckle[28,29] to directly probe surfaces. In this framework, the present study focuses on a new and simple laser-based method to detect dew on both hydrophobic and hydrophilic leaf surfaces based on the light reflection and in particular Heiligenschein phenomenon. It essentially intends to evaluate the sensitivity of such a method, in terms of surface coverage and delay of detection, in controlled lab conditions mimicking the generation of dew. In the ultimate vision of using our set-up in real open-field conditions, scanning over large surfaces and different configuration of leaves, we estimate the impact of a scanning measurement as well as of the angle of incidence of the probe beam on the surface.

II. METHODS

When light reaches the surface of water, it undergoes several processes simultaneously, including reflection, refraction, absorption, and scattering. Under particular circumstances (e.g. when the surface is hydrophobic), light can be strongly reflected because water forms spherical droplets at the surface of the material. This is called the Heiligenschein phenomenon.

A. Heiligenschein phenomenon

Heiligenschein is a phenomenon visible when light strikes a droplet-covered hydrophobic surface. Light is reflected towards its source thanks to refraction inside droplets and reflection onto the underlying surface (see Fig. 1). This results in a bright light seen if the object illuminated is observed from nearby the light source axis. A pioneer study[30] has isolated four parameters influencing the amount of light returning to the source : the intensity of the incident source, the sphericity of the drops, the surface reflectivity and the apparent surface coverage. A maximum of intensity for an incident angle of about 60° with respect to the normal to the surface was also predicted with a smooth surface with no rising leaf hairs. This phenomenon occurs on hydrophobic surfaces such as *Brassica napus* leaves and is not expected on hydrophilic surfaces like *Vitis vinifera* leaves (contact angle θ_c respectively of 113.55° ± 2.79°[31] and 62° ± 14°[32]).

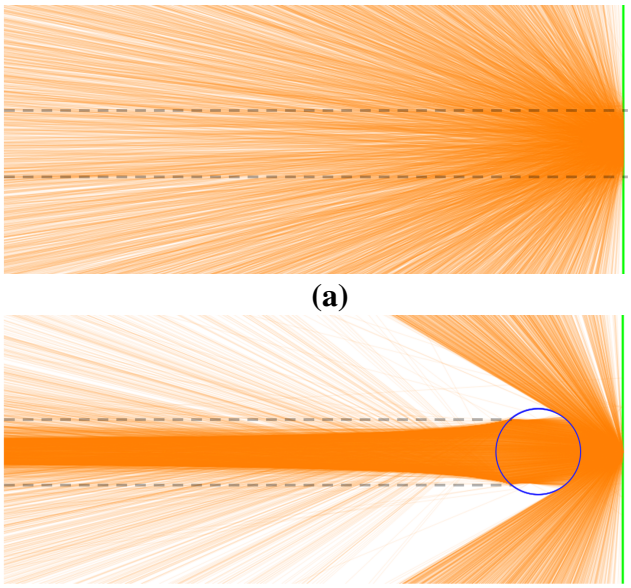

FIG. 1: **a)** Lambertian scattering by a leaf **b)** Heiligenschein phenomenon. Collimated light beam coming from the left (beam edges in semi transparent dash lines), is focused by the drop (in blue) and scattered by the leaf surface (in green) and re-focused by the drop. Scattered rays are in orange. This results in a very concentrated beam going back towards the source. The distance between the drop and the leaf has been chosen in order to have a strong Heiligenschein effect for the sake of clarity.

B. Experimental set-up

Figure 2 details the experimental set-up. A laser diode is a good choice as a low-cost source thanks to its intense and collimated beam characteristics. In the present case, we have chosen as a source, a 633nm CPS635R laser diode from ThorLabs with a 1.2 mW optical power. A beam of 1 cm in diameter at 1 m working distance is achieved by using a lens. Source fluctuations are monitored by a PM16-121 photodiode from ThorLabs coupled with a beam splitter to the source output. In our controlled experimental conditions, these fluctuations are negligible (<0.5%). Hence, the power monitoring has not systematically been done in order to simplify the analyses. For the detector, a 20 Mpx monochromatic CMOS camera manufactured by Basler has been chosen along with a V5024-MPZ (50mm objective) manufactured by Computar. This camera has a 8-bit depth. In the visible range (400-650 nm), the camera quantum efficiency is between 50% and 80 %. A 90° mirror is added in order to stack the camera field of view with the laser beam. Source and detector are assembled following a biaxial configuration and bound together using stainless steel rods. Distance between the laser beam center and the nearest point of the mirror is equal to 1 cm ± 1 mm. Equally, the distance from the laser beam center to the farthest point of the mirror is equal to 3 cm ± 1 mm. This corresponds to an angular deviation respectively equal to 0.57° ± 0.06° and 1.71° ± 0.06° at 1 m. Hence, conditions of Heiligenschein are respected using this configuration. Finally, a controlled-mirror using two ZST206 stepper motors and two KST101 controllers manufactured by Thorlabs allow changing the beam position on the leaf below the optical set-up.

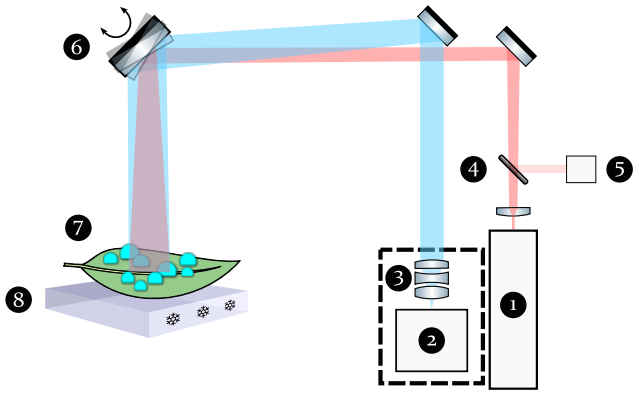

FIG. 2: Scheme of the experimental set-up. In red : Light forward path. In blue : Light backward path. **1** : Laser. **2** : CMOS sensor. **3** : Objective. **4** : Beam splitter. **5** : Power meter. **6** : Controlled mirror. **7** : Leaf. **8** : Cooling/heating Peltier module.

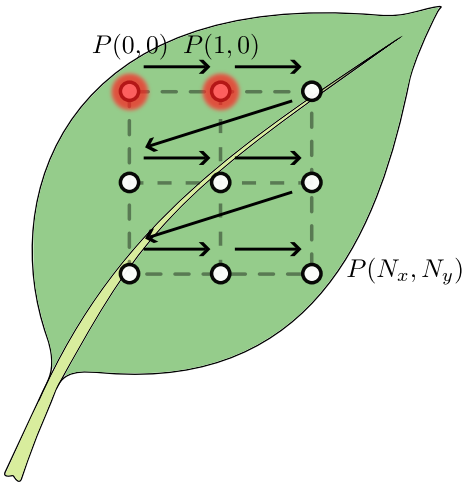

FIG. 3: Example of sequence of position in the scanning experiment. The laser beam is moved from $P(0,0)$ to $P(N_x,N_y)$ where N_x and N_y are the number of nodes in both directions.

The intensity received is the main signal to measure. In our case, using a monochromatic camera, the signal corresponds to the average of the intensity measured by each pixel.

Of prime importance in our protocol was the ability to generate dew on the leaf. For that purpose, the leaf was cooled down to the temperature required for water vapor condensation, depending on the ambient hygrometry using a cooling/heating Peltier module. The leaf to be cooled was placed horizontally on this plate. Weights were placed on different parts of the leaf to ensure a uniform contact with the plate for uniform cooling. The cooling temperature and the temperature ramp at the very surface of the leaf were controlled after a calibration linking the cooling plate temperature to the leaf temperature (see Supplementary Discussion). Air temperature and hygrometry were monitored using a weather station ($\pm$ 1°C for the temperature, $\pm$ 3% for the relative humidity, RH). A measure was done every five minutes by the station. In order to reduce uncertainties, a 5-points moving average of the weather station measurements has been used based on the fact that the experiment is performed in a temperature-controlled room. Thus, dew point temperature could be computed in order to know the moment where dew formation had started. To confirm the accuracy of the measurements obtained in a temperature-controlled room, additional measurements were conducted in a climatic chamber where both the humidity and temperature were regulated (see Supplementary Discussion). The laser was kept turned on during the experiment in order to have the most intensity-stabilized beam while the room was in the dark. Hydrophobic and hydrophilic species used during experiment were respectively grapevine (*Vitis vinifera*) and rapeseed (*Brassica napus*) leaves.

Once the experiment started, images were captured by the camera during $T_{acquisition} = 10\ \mu s$ every $T_{measure} = 5$ s. Meanwhile, the cooling plate was turned on after a predefined delay so that the first acquisition could serve as a reference background signal. During every image acquisition, plate temperature and laser intensity were measured. The time needed to do these tasks was estimated at 200 ms $\pm$ 10 ms. Besides, a commercial wetness sensor PHYTOS 31 commercialised by METER group coupled to a data logger from Weenat was added to the cooling plate. Measurements by this sensor are done based on relative permittivity modifications. Retrieved values are between 0 and 100% in steps of 10% corresponding to respectively a dry leaf surface (i.e. without water on its surface) and a water-saturated leaf surface. The sensor returned a value every hour. Data collected were used in order to have a reference with measurements made with our method. The temperature decrease was performed at two different speeds (6°C/min and 0.3°C/min). These two speeds are called respectively "fast" and "slow" in next sections. These values are discussed in section IV. The temperature decrease continued until the leaf temperature reached 8 °C $\pm$ 0.2 °C. When applicable, temperature returned to its initial value in order to have dew evaporation using the same temperature ramp.

C. Scanning and inclination influence set-up

To be closer to field conditions, some variables must be taken into account. First, in field, leaves have various orientations unlike our first set-up where the leaf was always orthogonal to incident laser beam. Second, if one wants to get local information at different locations, it is necessary to be able to scan an entire field with the laser beam. For that purpose, a controlled mirror was used to change the measurement area. This last point could allow our method to map an area in a field which would be a clear benefit compared to punctual leaf wetness sensors.

To study the influence of leaf orientation, the experimental method detailed previously was used again. However, the cooling plate was replaced by a 2-axis rotation stage manufactured by Stranda (see SF. 1 in Supplementary Figures). Here, the experiment aimed at quantifying how the leaf orientation affects the signal received by the camera when the leaf surface is wet or dry. Yet, the complexity of combining the cooling plate and the 2-axis rotation stage prevented their utilization at the same time. Hence, dew formation by cooling was replaced by water spraying to reproduce dew presence when the surface coverage was maximum. The deposited leaf could be oriented around θ and ϕ. These two angles varied between $\pm$ 45° in both directions with a 2° and 10° resolution for acquisitions respectively on dry and wet leaf. To reduce water evaporation during the experiment, wet leaves that were not temperature-controlled had limited angular resolution and acquisition time. The case where the leaf was horizontal corresponded to our origin (0°,0°) in the two directions with an orthogonal incident laser beam. A first acquisition was realized on the dry leaf by modifying the angle value by increments. Then, water was sprayed on the leaf until the maximum surface coverage ε_2 was approximately reached for the contact angle θ_c corresponding to the studied leaf (Eq. 1[33]) and finally a second acquisition was done. These steps were repeated ten times so variations due to leaf surface roughness were averaged out.

$$\varepsilon_2 \approx 1 - \frac{\theta_c}{180} \quad (1)$$

For the scanning experiment, the measurement area was changed using the controlled mirror (mirror 6 in Fig. 2) following predefined positions. Changing the measured area limits leaf surface roughness effects (i.e. leaf veins) and avoids delaying the detection of dew formation due to heterogeneity resulting from the leaf surface roughness. The mirror mount allowed a $\pm$ 6° range which corresponds to a $\pm$ 10 cm at a distance of 1 m with a maximum resolution of 150 μm.

Positions were defined by dividing the two dimensional travel distance in the leaf plane by the number of nodes wanted. Positions were traveled sequentially during all the acquisition time (Fig. 3). To ensure acquisition periodicity, a variable buffer time was added, which was adjusted at each increment based on the necessary time spent moving the measurement area during the previous increment, due to differences in distance between positions (such as when the mirror returns to the first position). Here, the beam went by nine equidistant positions arranged on a three-by-three grid. The distance between each position was 3 cm.

D. 2D ray-tracing simulations

In order to specify which parameter the signal is sensitive to, numerical Monte-Carlo simulations of ray tracing were performed. These simulations reproduced the dew formation process on a leaf associated with the incidence of light rays from a laser source. Details on the simulations are available in Supplementary Discussion. In the case of hydrophobic surface (i.e. the simulated drops are spherical), the minimum radius of the simulated drops must measure at least 1 μm when using a 633nm laser in order to be in the geometrical optics regime[34]. Also, for the sake of simplicity, we assume that we were in the case of geometric optics for hydrophilic surfaces. Therefore, this condition gave us the lower bound for our simulation in terms of object size. Moreover, by considering, as a first approximation, the optical properties of leaves and water as homogeneous and isotropic, the experimental conditions can be reduced to a two-dimensional system. We started by defining a scene including one or more of these objects: laser, camera and leaf. The ambient temperature T, the temperature at which the leaf was cooled T_{leaf} and the relative humidity RH can also be defined. Thus, the condensation rate per unit area $\dot{h}$ was computed according to Eq. 2[33]. We set a constant $\dot{h}$ for the whole experiment. The set of parameters defining each of these objects as well as the constants used are described in Supplementary Tables.

$$\dot{h}(T, T_{leaf}, RH) = \frac{(p_w(T,RH) - p_s(T_{leaf}))a_w(T,RH)}{\rho_w} \quad (2)$$

with p_w the partial pressure of water vapor, p_s the saturation vapor pressure of water and ρ_w the density of water. Similarly, a_w the transfer coefficient of water vapor is defined by Eq. 3 :

$$a_w = \frac{r_a \rho_a(T) D}{r_v \zeta p_m(T,RH)} \quad (3)$$

With r_a the specific constant of dry air, r_v the specific constant of water vapor, ρ_a the density of air, D the mutual air/water diffusion coefficient, ζ the thickness of the diffusion boundary layer and p_m the atmospheric pressure.

Thus, dew drop formation and growth were simulated at the surface of the defined leaf by computing $R_i(t)$ the radius of the drop at time t. In order to be as close as possible to the real conditions, the growth of the drops followed the growth law of an isolated drop (i.e. proportional to $t^{1/3}$, Eq. 4) and then changed once coalescence events occurred (i.e. proportional to t, Eq. 5)[33].

$$R_i(t) = \left[\frac{\dot{h}}{\pi f(\theta_c)} \langle d \rangle^2 \right]^{1/3} t^{1/3} \quad (4)$$

With $\langle d \rangle$ the average distance between the drops. In the same way, in the coalescence regime,

$$R_i(t) = \frac{\dot{h}}{\varepsilon_2 f(\theta_c)} t \quad (5)$$

With ε_2 the water surface coverage of the leaf and where,

$$f(\theta_c) = \frac{2 - 3\cos(\theta_c) + \cos^3(\theta_c)}{3\sin^3(\theta_c)} \quad (6)$$

With θ_c the contact angle of the drop with the leaf.

Simulations were conducted independently of experiments using fixed parameters. They were then compared to the experimental results by normalizing the simulation result to the lowest and highest experimental values.

III. RESULTS

A. Single-point static measurement

1. *Hydrophobic leaf*

Figure 4 shows the moving average of the pixel average value based on 20 points (i.e 100 s of measurement), during a fast cooling of a rapeseed leaf with a static measurement area. The moving standard deviation at $\pm 2\sigma$ of the measurements is represented by curves in light gray. The pixel average value is normalized to the first value displayed for analysis and clarity purposes. For the same reason, the moment when the leaf temperature drops below the dew point temperature is symbolized by the vertical blue line. The uncertainty related to this threshold is symbolized by the vertical blue dotted lines in Fig. 4b. The signal can be divided into three parts : a stable first part, then an ascending part that reaches in the final

part a constant $M_{\infty,rapeseed,fast}$ value corresponding to a pixel value higher than in the first part. The first part corresponds to the time period where the leaf is still mostly dry. Indeed, the temperature of the leaf decreases after 10 minutes and reaches the dew point, approximately 3 minutes later, actually in the uncertainty range of [12.82 min; 13.50 min]. During all this time, the value of the average pixel remains stable. Once the leaf temperature has passed under the dew temperature threshold, the pixel average value increases sharply and then reaches a plateau corresponding to an increase of the measured reflected light intensity of about 39% larger than the initial signal. The signal value remained within the interval [1.37; 1.40]. The presence of water is confirmed by the wetness sensor.

To get more insight into the possible mechanism responsible for the signal increase, we have performed ESEM (Environmental Scanning Electron Microscopy) experiments on leaves (Pictures 1,2 and 3 in Fig. 4c). These pictures are chosen at three distinct phases of the dew formation process. These phases are different from the three parts invoked previously. Complete movies of condensation with ESEM are available in Supplementary Videos. During water condensation, the drops remain spherical and their contact angle on the hydrophobic leaf remains constant. Also, there are progressively less and less drops but with increasing radii. These observations are consistent with the nucleation and growth process of dew formation. The presence of spherical drops is also consistent with the Heiligenschein phenomenon explaining the reflected intensity increase observed in our experiment. Besides, the uncertainty increases in the presence of water compared to the dry leaf. Therefore, the moving standard deviation could also be used to determine accurately the timing of water appearance.

In Figure 4a is also presented the smoothed signal obtained from the Monte-Carlo simulation of ray tracing. The maximum signal is normalized to the maximum experimental signal. The good agreement between experiment and simulation further confirms that the Heiligenschein effect reproduces quite well our observations. Both the simulated and observed signals follow a sigmoid function. This statement goes to show that our sensor mostly measures the surface coverage. In the peculiar case of the hydrophobic rapeseed leaf, with a critical angle of $\theta_c = 113.55° \pm 2.79°$[31], the maximum surface coverage predicted by Eq. 1 is about 0.37. If one takes a close look at the region where dew formation initiates, one can notice a discrepancy between the experimental and simulated signals (Fig. 4b). This suggests a condensation rate that fluctuates over time contrary to what was adopted for the simulations. This could also come from the heat released during water vapor condensation on the leaf, delaying further condensation of water to form more droplets.

Subsequently, the dew point detection threshold is determined as follows. When the lowest value of the uncertainty interval of the dew point threshold (i.e. left blue dashed line) is crossed, the high uncertainty value of the signal becomes our reference. This reference is the value that the averaged signal must exceed in order to conclude that dew is forming. Thus, the delay between the appearance of the dew and its de-

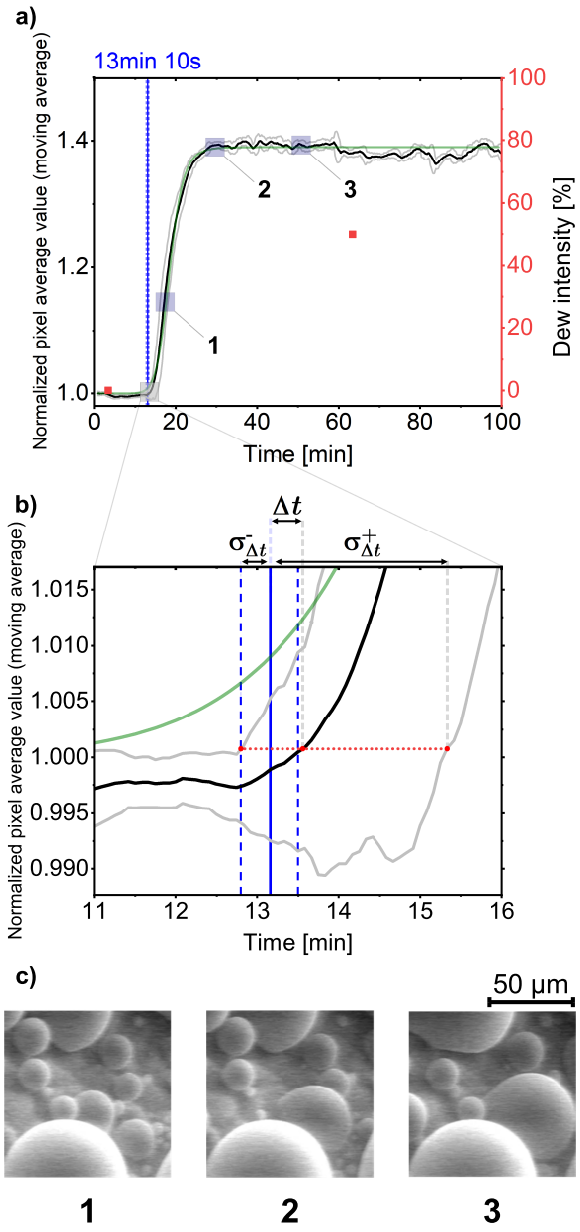

FIG. 4: **a)** Evolution of the pixel average value (moving average) with the fast cooling of a hydrophobic rapeseed leaf (*Brassica napus*) and a static measurement area (black). The moving standard deviation at $\pm 2\ \sigma$ of the measurements is represented by the gray curves. The signal obtained by numerical simulation is represented in green. The vertical blue line and text represent the moment when the leaf temperature drops below the dew point. The blue dotted lines represent the uncertainty in determining this instant. The results of the simulations are plotted in the signal fluctuation interval. The value of an average pixel is normalized to the first value of the measurement series for analysis and clarity purposes. The measurement points of the leaf wetness sensor are represented by red squares. **b)** Zoom of graph a). Representation of the determination of the dew formation detection delay determination and its uncertainties. **c)** ESEM observations illustrating dew formation of graph a).

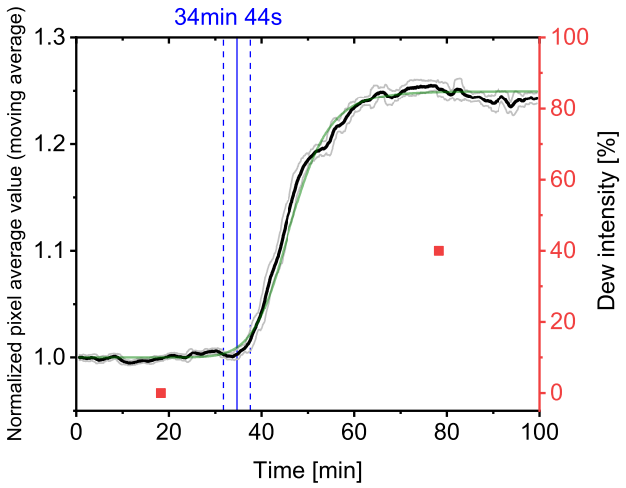

FIG. 5: Evolution of the pixel average value (moving average) with the slow cooling of a hydrophobic rapeseed leaf (*Brassica napus*) and a static measurement area (black). The moving standard deviation at $\pm 2\ \sigma$ of the measurements is represented by the gray curves. The signal obtained by numerical simulation is represented in green. The vertical blue line and text represent the moment when the leaf temperature drops below the dew point. The blue dotted lines represent the uncertainty in determining this instant. The results of the simulations are plotted in the signal fluctuation interval. The value of an average pixel is normalized to the first value of the measurement series for analysis and clarity purposes. The measurement points of the leaf wetness sensor are represented by the red squares.

tection (or dew formation detection delay) $\Delta t^{rapeseed,fast}$ can be evaluated. In the fast-cooling case (Fig. 4), it is evaluated at 0.5 min in the uncertainty range of [-0.36;2.16]. Based on the simulation results, this corresponds to a surface coverage of about 1.2% [0.7;3.4] and an average droplet radius of about 11.0 μm in the uncertainty range of [7.8;21.4]. Compared to the leaf wetness sensor, the measurements made by our method provide more accurate information at a higher frequency.

In the case of a slow cooling, the same trend is found (Fig. 5). However, the maximum $M_{\infty}^{rapeseed,slow}$ reaches about 1.25 with an uncertainty interval of [1.24;1.26] after the surface coverage stabilization. A fluctuation in the value of M_{∞} appears as water does not form uniformly over the entire surface of the leaf (c.f. section IV). Similarly, $\Delta t^{rapeseed,slow}$ is evaluated. It is estimated at 0.6 min in the uncertainty range of [-2.93;1.69]. The dew formation detection delay is quite equivalent compared to $\Delta t^{rapeseed,fast}$. However, the uncertainty related to the determination of this value increases. Indeed, the uncertainty of the dew temperature being constant, a slower cooling rate induces a larger uncertainty on the dew formation detection delay. Using the simulations, the average droplet radius at $\Delta t^{rapeseed,slow}$ is about 18.2 μm in the uncertainty range of [10.1;22.2] and the surface coverage is about 2.6% in the uncertainty range of [1.0;3.5].

To ensure that the main variable influencing the signal is the water coverage on leaf surface, the leaf has been heated back to its temperature before cooling using the same temperature ramp (Fig. 6). The moment when the temperature was above the dew temperature, corresponding to the moment when the dew evaporation started, is indicated by the purple solid and dashed lines. After this threshold crossing, the signal decreases and returns to its normalization value as expected. This return is faster than during the rise to the plateau during dew formation respectively lasting roughly 50 minutes and 80 minutes in the case of this acquisition. The criterion used to evaluate the dew formation detection delay $\Delta t^{rapeseed}$ above can be applied in order to have the dew evaporation detection delay $\Delta t_{ev}^{rapeseed}$. These two delays are evaluated at respectively 0.44 min in the uncertainty range of [-3.19;1.44] and 3.71 min in the uncertainty range of [3.05;6.12].

2. *Hydrophilic leaf*

Three steps in the evolution of the pixel average value are also present in the case of a hydrophilic surface, as shown in Figure 7. Here, the experiment shown is performed on a grapevine leaf with the fast cooling rate. In contrast to the previous section, the overall evolution of the signal is decreasing and thus the value of $M_{\infty}^{grapevine,fast}$ is lower than the normalization value. After stabilization at the end of the experiment, the signal reaches 0.538 (uncertainty interval of [0.536-0.540]) which is almost half of the initial signal. The presence of water is also confirmed by the wetness sensor. Numerical simulations are still in progress and do not allow us to conclude on the mechanism involved here. Nonetheless, preliminary simulation results provide hypothesis presented in the Discussion section. However, the signal trend shows that the Heiligenschein effect is non-existent in this configuration. ESEM grapevine observations (Fig. 7) show that water condensation on a hydrophilic leaf leads to a more heterogeneous situation than for the hydrophobic leaf. Indeed, water films of complex shape coexist with simple water lenses. In the case of the hydrophilic grapevine leaf, drops form a water film rather than spherical drops. Light may be more strongly dispersed when water is spread on the leaf surface than when it is dry. The dew detection threshold can still be determined by using the method applied previously but the signal decay requires the criterion to be adapted. In the hydrophilic case, it is the value of the low uncertainty of the signal that is our reference. In the same way as before, $\Delta t^{grapevine,fast}$ is evaluated at 0.05 min (or 3s) in the uncertainty range of [-0.51;1.63]. The standard deviation of the measurements remains relatively constant during the whole experiment, contrary to what was observed for the hydrophobic leaf.

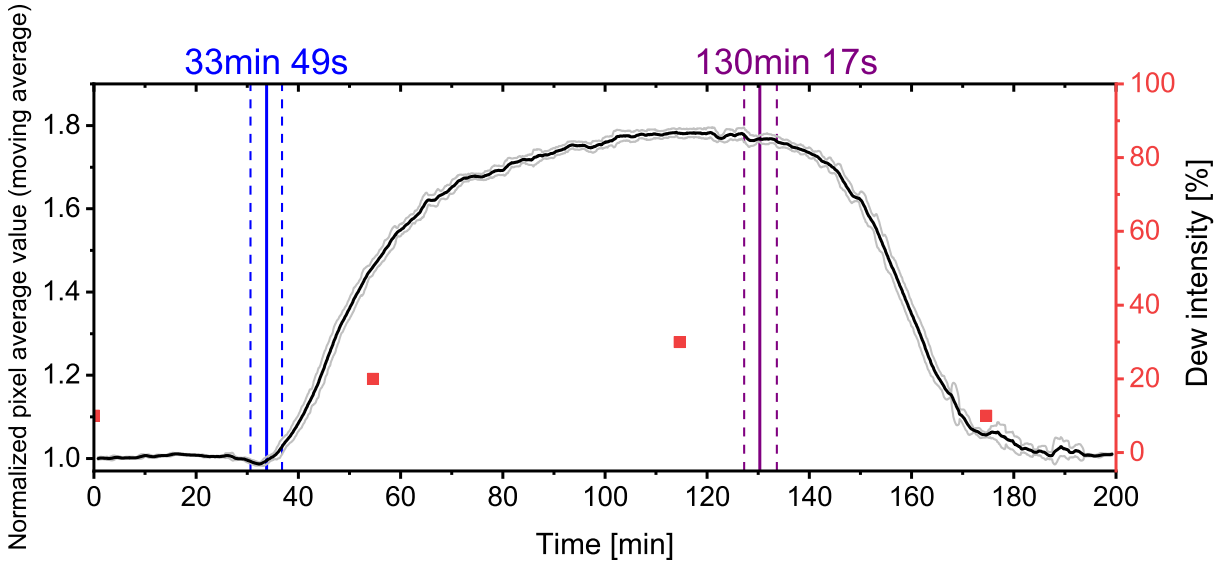

FIG. 6: Evolution of the pixel average value (moving average) with the slow cooling of a hydrophobic rapeseed leaf (*Brassica napus*) and a static measurement area (black) followed by a slow heating using the same temperature ramp. The moving standard deviation at $\pm 2\ \sigma$ of the measurements is represented by the gray curves. The vertical blue (or purple) line and text represent the moment when the leaf temperature goes below (or surpasses) the dew point. The blue (or purple) dotted lines represent the uncertainty in determining this instant. The value of an average pixel is normalized to the first value of the measurement series for analysis and clarity purposes. The measurement points of the leaf wetness sensor are represented by the red squares.

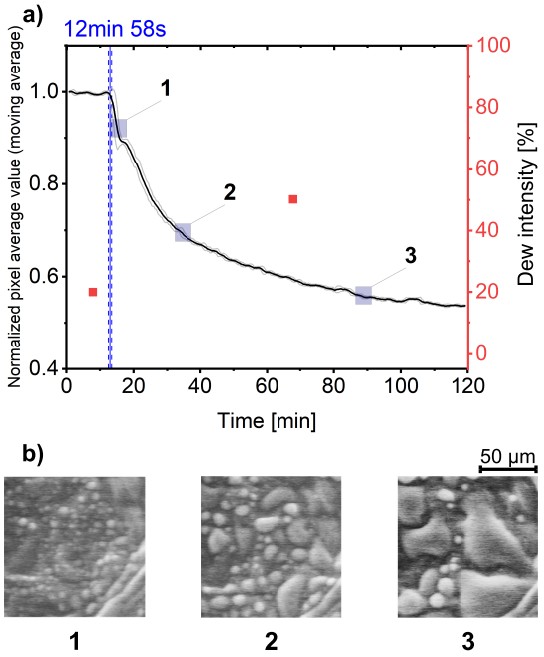

FIG. 7: **a)** Evolution of the pixel average value (moving average) with the fast cooling of a hydrophilic grapevine leaf (*Vitis Vinifera*) and a static measurement area (black). The moving standard deviation at $\pm 2\ \sigma$ of the measurements is represented by the gray curves. The vertical blue line and text represent the moment when the leaf temperature drops below the dew point. The blue dotted lines represent the uncertainty in determining this instant. The value of an average pixel is normalized to the first value of the measurement series for analysis and clarity purposes. The measurement points of the leaf wetness sensor are represented by the red squares. **b)** ESEM observations illustrating dew formation of a).

Figure 8 shows two cases of slow cooling of a hydrophilic leaf with a static measurement area at two different locations on the same leaf. The same evolution as in Figure 7 is visible in the first case (Fig. 8a). Indeed, a decrease of the signal is visible as soon as the leaf temperature goes under the dew point. At the end of the experiment, $M_{\infty}^{grapevine,slow}$ is 0.59 in the uncertainty range of [0.604;0.577], which is relatively close to what was found for $M_{\infty}^{grapevine,fast}$. $\Delta t^{grapevine,slow}$ is evaluated at -24 s in the uncertainty range of [-2.90;1.15]. Here, the delay is negative which is consistent given the uncertainties but shows the limit of the chosen criterion. On the other hand, Figure 8b shows that the signal trend can be totally different depending on the position of the laser beam on the leaf in the case of slow cooling. This time, five steps can be distinguished on the graph. In the first part, as in the case of the hydrophobic leaf, the signal is stable around the normalization value, corresponding to the dry leaf. The signal increase before the onset of the dew formation is not explained (see Discussion). As soon as the leaf temperature falls below the dew point, the signal increases and reaches a constant value comparable to what is observed under the same conditions on the hydrophobic leaf. Finally, the signal decreases and reaches $M_{\infty}^{grapevine,slow,bis}$ lower than the one at the beginning of the experiment. The value of this final constant corresponds to a decrease of 6% (uncertainty range : [0.931;0.945]).

By analogy with the hydrophobic case, we assume that the increasing part of the signal is explained by the Heiligenschein effect. In this scenario, at this location on the leaf, mostly spherical drops would form. This is corroborated by the high intensity areas visible in the comparison between raw

images extracted from the experiment with the hydrophobic leaf and this experiment (see SF. 2 in Supplementary Figures). Then, by analogy with the observations made on the other hydrophilic leaves, we find a decrease in the signal, related to very heterogeneous forms of drops.

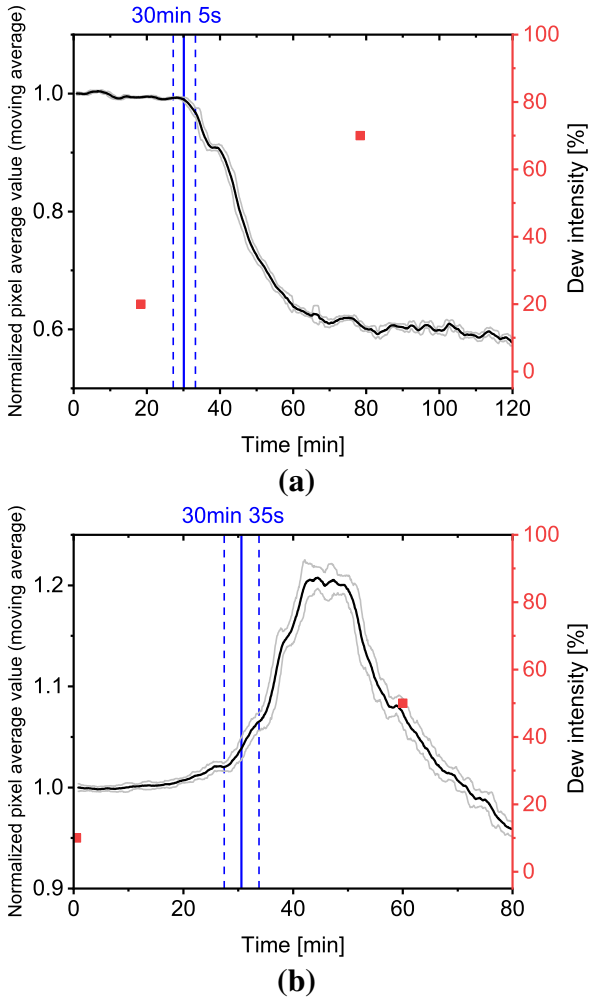

FIG. 8: Evolution of the pixel average value (moving average) with a slow cooling of a hydrophilic grapevine leaf (*Vitis vinifera*) and a static measurement area (in black) at two different measurement positions of the same leaf. The moving standard deviation at $\pm 2\sigma$ of the measurements is represented by the gray curves. The vertical blue line and text represent the moment when the leaf temperature drops below the dew point. The value of an average pixel is normalized to the first value of the measurement series for analysis and clarity purposes. The leaf wetness sensor measurement points are represented by the red squares.

Therefore, a measurement at two different times can give the same value while the leaf is in two different states. This is consistent with the observation of the various forms of the water films described before. Finally, $\Delta t^{grapevine,slow,bis}$ is found and estimated at -1.83 min in the uncertainty range of [-3.15;-0.75]. Here, the negative value of both uncertainty limits suggests an error in the determination of the leaf temperature or the criterion invalidity.

In the same way than in the hydrophobic leaf case, the leaf has been heated back to its initial temperature before cooling after dew formation and signal stabilization (Fig. 9). Interestingly, the signal rises and returns to its normalization value with remarkably high chaotic peaks just before stabilization. This might be related to the peak observed in Figure 8b at the beginning of the dew formation process and explained above. The dew formation detection delay Δt^{vine} and the dew evaporation detection delay Δt_{ev}^{vine} are evaluated at respectively 0.12 min (uncertainty range : [-2.91;1.04]) and 2.91 min (uncertainty range : [-2.87;4.16]).

B. Scanning and leaf inclination influence

1. *Scanning of the hydrophobic leaf*

The same observations made during the static experiment on the rapeseed leaf can be done while scanning the leaf (Fig. 10). Indeed, the three steps are clearly visible. On the other hand, $M_{\infty}^{rapeseed,scan}$ is more than three times higher than the normalization value used as a reference when the leaf is still dry (3.52, uncertainty range : [2.99-4.05]). This is in sharp contrast to the 40% signal increase observed above with the static measurement area. As with Figures 4 and 5, the heterogeneity of water formation on the leaf helps to explain this higher value. Moreover, it gives an upper limit to the influence of the Heiligenschein effect on the reflected signal. The high frequency oscillations that can be observed in the signal are due to the change of measurement point following a scanning loop as explained before. The retrieved values of $\Delta t^{rapeseed,scan}$ is 2.22 min in the uncertainty range of [-3.70;6.97]. Compared to $\Delta t^{rapeseed,slow}$ determined during the slow cooling with a static measurement, scanning the leaf delays the dew detection. The mean radius and surface coverage at $\Delta t^{rapeseed,scan}$ are evaluated at 13.1 μm in the uncertainty range of [3.3;35.0] and 1.6% in the uncertainty range of [0.2;6.6] respectively. Overall, the evaluated values of mean radius and surface coverage are relatively close to the static measurement. However, the uncertainty in these estimates increases with slower temperature cooling and with the scanning. All values extracted from the data during the experiment with the rapeseed leaf are grouped in Table I.

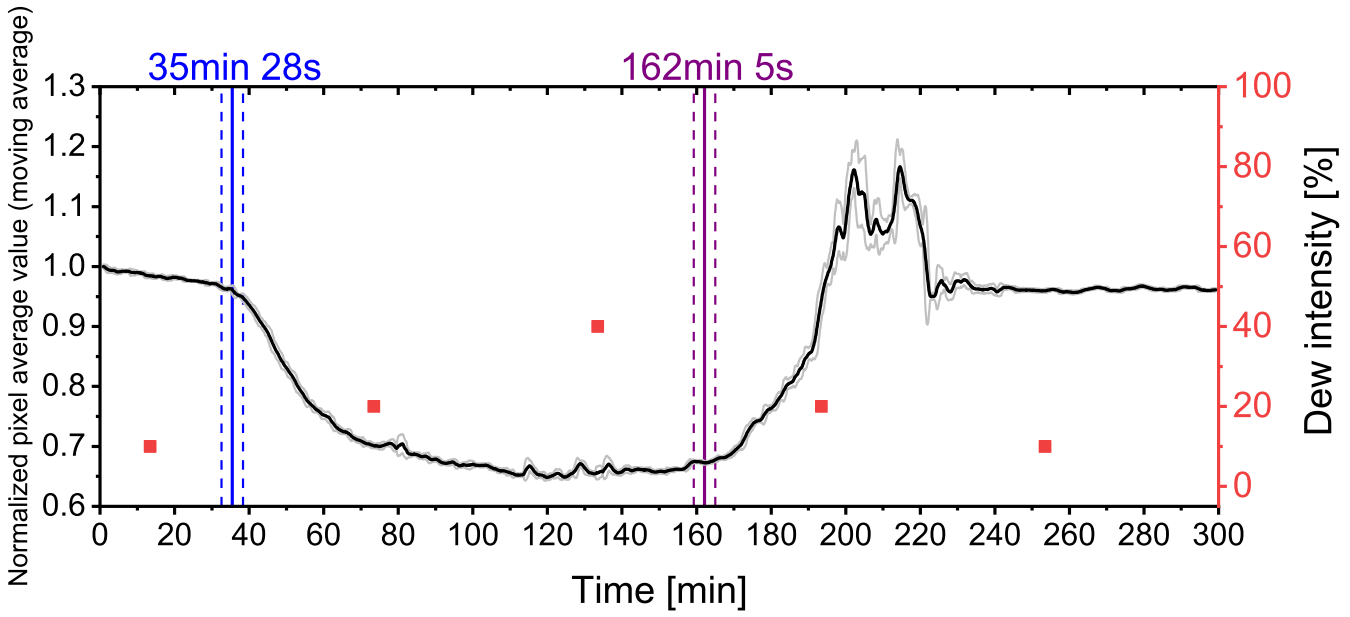

FIG. 9: Evolution of the pixel average value (moving average) with the slow cooling of a hydrophilic vine leaf (*Vitis Vinifera*) and a static measurement area (black) followed by a slow heating using the same temperature ramp. The moving standard deviation at $\pm 2\ \sigma$ of the measurements is represented by the gray curves. The vertical blue (or purple) line and text represent the moment when the leaf temperature goes below (or above) the dew point. The blue (or purple) dotted lines represent the uncertainty in determining this instant. The value of an average pixel is normalized to the first value of the measurement series for analysis and clarity purposes. The measurement points of the leaf wetness sensor are represented by the red squares.

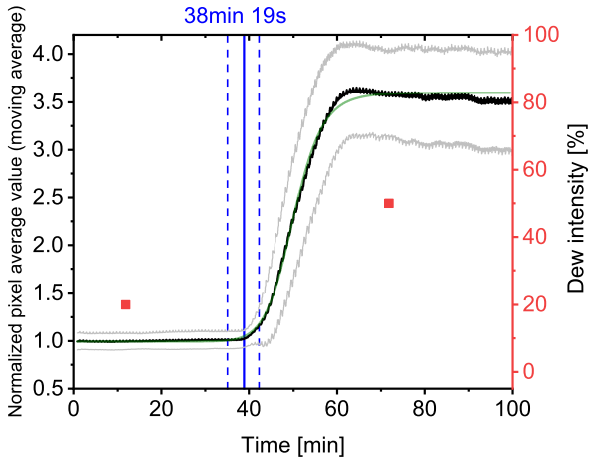

FIG. 10: Evolution of the pixel average value (moving average) with the slow cooling of a hydrophobic rapeseed leaf (*Brassica napus*) and a scanning measurement (black). The moving standard deviation at $\pm 2\ \sigma$ of the measurements is represented by the gray curves. The signal smoothing obtained by numerical simulation is represented in green. The vertical blue line and text represent the moment when the leaf temperature drops below the dew point. The blue dotted lines represent the uncertainty in determining this instant. The results of the simulations are plotted in the signal fluctuation interval. The value of an average pixel is normalized to the first value of the measurement series for analysis and clarity purposes. The measurement points of the leaf wetness sensor are represented by the red squares.

2. *Scanning of the hydrophilic leaf*

With the use of a scanning measurement (Fig. 11), the two cases described in Figure 8 are found. Figure 11a shows a signal decrease similar to the one observed in Figure 8a. The value of $M_{\infty}^{grapevine,scan}$ corresponds to a 0.73 times weaker signal compared to the normalization value. The dispersion of the data when the hydrophilic leaf is dry is comparable to that of the hydrophobic leaf ($\pm$ 10%) (Fig.10). On the other hand, this dispersion decreases at the beginning of the dew formation and then increases. In contrast to this case, Figure 7 showed a constant dispersion over time while water was present on the leaf surface. This dispersion depends in part on the measurement area. Consequently, if dew detection has to be performed scanning across a field, it might be preferable to use the moving standard deviation as the sensing signal instead of the moving average signal intensity. Next, $\Delta t^{grapevine,scan}$ is retrieved and evaluated at 19.35 min (uncertainty range : [-3.22; 32.26]). This value confirms the disadvantage of the scanning measurement which delays dew detection using our criterion.

TABLE I: Summary of the values extracted from the experiments on the hydrophobic leaf. The values in square brackets correspond to the uncertainties determined from the standard deviation at $\pm 2\sigma$ of the experimental signals.

	Detection delay [min]	**Minimum average detectable droplet radius [μm]**	**Minimum detectable surface coverage [%]**
Fast cooling	0.05 [-0.51;1.63]	11.0 [7.8;21.4]	1.2 [0.7;3.4]
Slow cooling	0.6 [-2.93;1.69]	18.2 [10.1;22.2]	2.6 [1.0;3.5]
Scan	2.22 [-3.70;6.97]	13.1 [3.3;35.0]	1.6 [0.2;6.6]

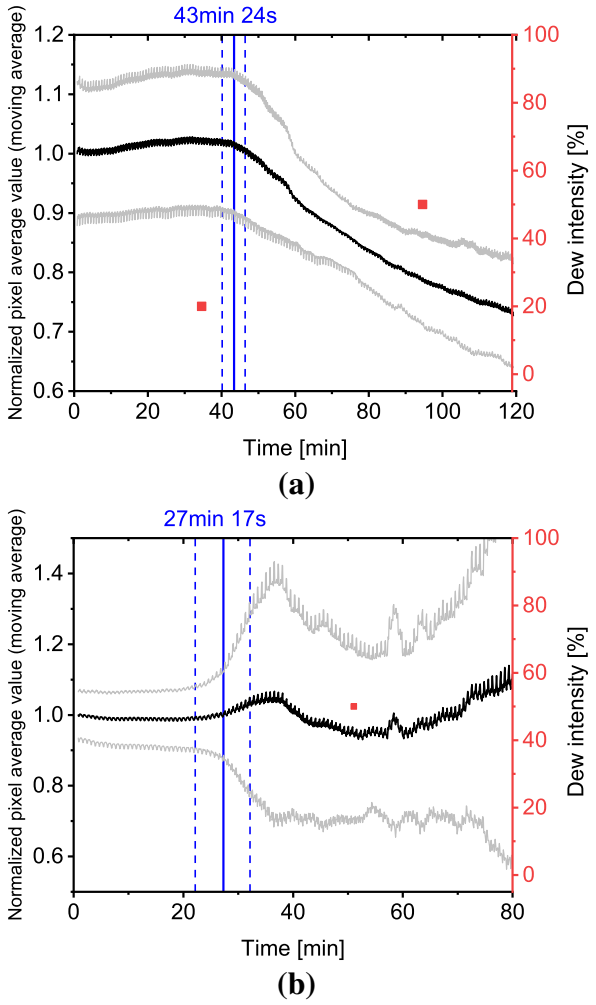

FIG. 11: Evolution of the pixel average value (moving average) with a slow cooling of a hydrophilic grapevine leaf (*Vitis vinifera*) and a scanning measurement (in black) using two different sequences of measurement positions of the same leaf. The moving standard deviation at $\pm 2\sigma$ of the measurements is represented by the gray curves. The value of an average pixel is normalized to the first value of the measurement series for analysis and clarity purposes. The leaf wetness sensor measurement points are represented by the red squares.

Finally, Figure 11b is a good synthesis of the previous figures. Indeed, the moving average of the signal shows that the majority of the measurement is similar to the one presented in Figure 8b characterized by an initial increase of the signal followed by a decrease. However, the high uncertainty of the signal goes to show that as the laser beam scans over several areas, it might encounter different situations, some similar to the case of Figure 8a and others to Figure 8b. The high uncertainty is representative of the heterogeneity described in ESEM observations before. Therefore, we expect the signal to be a mixture of these two distinct behaviors. Here, the dew detection criterion is not applicable because of the strong dispersion of the signal throughout the experiment. Thus, it is necessary to revise this criterion or the way it is used in order to cover all possible cases. As before, all values extracted from the data are grouped in Table II.

TABLE II: Summary of the values extracted from the experiments on the hydrophilic leaf. The values in square brackets correspond to the uncertainties determined from the standard deviation at $\pm 2\sigma$ of the experimental signals.

	Detection delay [min]
Fast cooling	0.03 [-0.76;1.43]
Slow cooling	-0.4 [-2.90;1.15]
Slow cooling bis	-1.83 [-3.15;-0.75]
Scan	19.35 [-3.22; 32.26]
Scan bis	-

3. *Leaf inclination influence*

Regarding leaf inclination influence, some observations are evenly visible on both leaves while others are specific to each leaf. Figure 12 and 13 show the normalized average pixel value in function of the inclination angles θ and ϕ and surface water presence (in blue) or absence (in green). Semi-visible curves stand for the 2σ standard deviation of experimental data. They are not shown in Figure 12c and 13c for the sake of clarity.

For the hydrophobic leaf, wet or dry, a symmetry is visible around the origin (0°,0°) indicating that the leaf is a uniform scattering surface. This point is chosen as the reference value for normalization except in Figure 12b where the maximum is found at the highest angles. Also, the dry hydrophobic leaf shows a signal decrease around the origin. When wetting the hydrophobic leaf, this point is a minimum. Yet, this minimum is 12.3% (in the uncertainty range of [0.98;1.24]) higher than the corresponding normalization dry-leaf value (see Fig. 12c). We retrieve there the results shown in the previous section where a higher signal is found with wet hydrophobic leaves thanks to the Heiligenschein phenomenon. Besides, as the incident angle increases, the ratio of the wet leaf signal to the dry leaf signal increases, reaching a record value of 4 for the largest angles (see Fig. 12c). This is fairly in accordance with

the Heilingenschein phenomenon that is expected to reach a maximum around an inclination angle of 60°[35]. It would be interesting to extend the angles used in this experiment to check this hypothesis on an hydrophobic leaf. Even though the signal generally increases as the incident angle increases, one may notice that at the orientation (45°,45°), the signal is actually rather low. This signal decrease at (45°, 45°) does not seem significant and would rather point to an artefact in the conduct of the experiment.

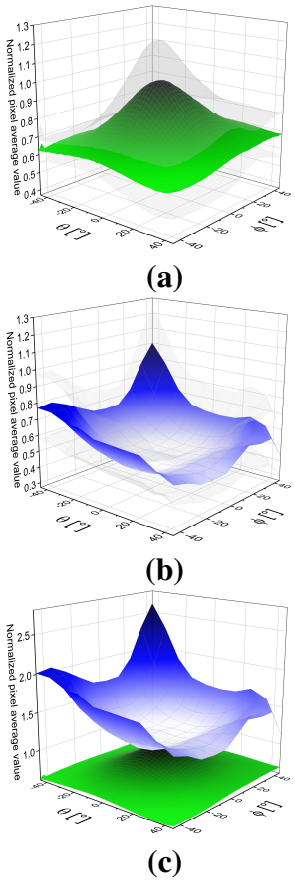

FIG. 12: Pixel average value as a function of θ, ϕ angles for a hydrophobic leaf (*Brassica napus*). The standard deviation at $\pm 2\sigma$ of the measurements are represented by the semi-transparent curves. **a)** Dry hydrophobic leaf. **b)** Wet hydrophobic leaf. **c)** Combination of a) and b). The intensity is normalized to the maximum value of the dry leaf experiment.

For the dry hydrophilic grapevine *Vitis Vinifera* leaf (Fig. 13), whether the leaf is dry or wet, a decrease of the signal around the origin (0°,0°) is visible. However, when the leaf is wet, the maximum signal value is roughly 20% (in the uncertainty range of [0.71;0.89]) lower than the normalization dry-leaf value. As in section III A 2, we suggest that water scatters the incident light. The average pixel value for wet leaf compared to the dry leaf can be 50% smaller for higher inclination angles. This experiment shows that the observations done in previous sections could be sensitively amplified thanks to variation in leaf inclination angles. In a more general

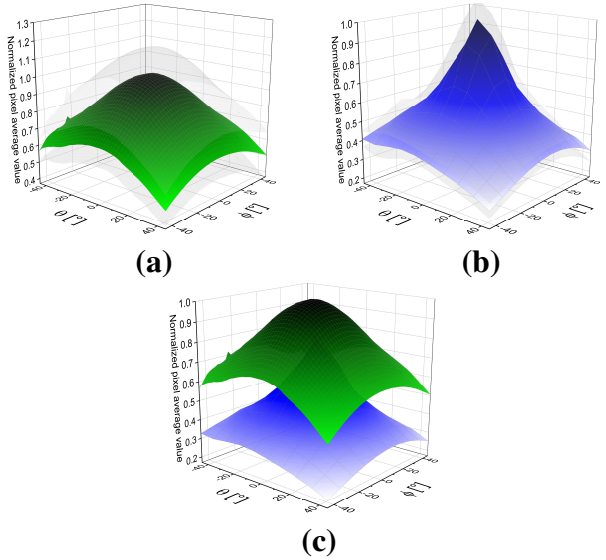

FIG. 13: Pixel average value as a function of θ, ϕ angles for a hydrophilic leaf (*Vitis Vinifera*). The standard deviation at $\pm 2\sigma$ of the measurements are represented by the semi-transparent curves. **a)** Dry hydrophilic leaf. **b)** Wet hydrophilic leaf. **c)** Combination of a) and b). The intensity is normalized to the maximum value of the dry leaf experiment.

way, increasing the number of iterations of the experiment as well as controlling the rotation stage temperature where the leaf is deposited could reduce the uncertainty of these results while increasing angular resolution for wet leaf experiment.

IV. DISCUSSION

The purpose of this proof of concept is to develop a device used in agricultural field, more demanding than our indoor controlled conditions. It is therefore necessary to study the limitations of our protocol with respect to this final application.

The determination of the dew detection threshold as detailed in sections III A 1 and III A 2 could be improved. In fact, it relies mainly on the calibration made in order to measure the leaf temperature from the temperature of the cooling plate (see Supplementary Discussion). The temperature measurement by the thermal camera varies from one leaf to another but also between different areas of the same leaf. Heterogeneity in the composition of the leaf (depending on its age, the area considered) implies a difference in the local thermal resistance[36]. Also, the curvature and leaf imperfections prevent it from being uniformly in contact with the cooling plate. Consequently, this calibration could be improved by an average over several iterations. This would allow a better precision on the determination of the dew detection threshold. Similarly, the dew detection criterion in itself could be refined. As a general observation, it seems to work well with a static measurement and a fast temperature gradient but could be improved for a scanning measuring point on a hydrophilic leaf. This comes

from the higher signal fluctuation induced when using a scanning measurement. The use of the moving standard deviation variation could improve this criterion and, ultimately, our detection.

We also assess signal variations that may occur at the start or end of experiments when condensation is not present. The slight decrease has been reproduced by cooling a grapevine leaf while keeping it above the dew temperature so that there is no condensation as corroborated by the commercial wetness sensor (see SF. 3 in Supplementary Figures). This provides evidence that the observed effect is specific to the leaf. Hence, the most likely hypothesis suggests that leaf reflectance is altered by cooling, and that the degree of alteration varies depending on the observed area of the leaf, such as the veins or the foliar area. Besides, leaf reflectance variation with its temperature has already been studied and has been used to determine specific plant characteristic[37,38]. However, additional experiments are needed to evaluate this hypothesis.

Concerning the leaf wetness sensor, the hourly measurement only indicates the presence or absence of water on the leaf surface under our experimental conditions. As seen in the previous figures, the maximum value never reaches 100% when the sensor is completely covered with water. Indeed, the sensor needs a few hours before reaching its saturation value, which is more in line with the real conditions of use. In the same way, according to the technical documentation, a measurement between 0% and 20% is in the fluctuation range of the sensor and is thus not significant. Finally, the measurement cannot be triggered manually with our data logger, which explains the inconsistency in the the number of measurements from this sensor in our experiments. Our indoor experiment requires a more precise way to measure leaf wetness in order to calibrate our sensor under development. Regarding the technical capabilities of the reference sensor[39], the leaf wetness duration is underestimated by five minutes. Compared to the different dew detection delays found above, our sensor equals or is well under these five minutes except for the measurement on the hydrophilic surface with a scanning measurement. In the case of a temperature gradient similar to that in the field and combined with a better dew temperature determination, the sensor could also maintain this delay under five minutes. Finally, our sensor gives, at least, the same amount of information than a resistivity leaf wetness sensor but with the added possibility of remote wetness mapping with a single sensor.

For practical reasons, the dew creation process is faster in our experiment than in reality. Indeed, the natural process is around 1°C/h or 0.017°C/min at night in dry weather and without wind[40]. This represents a speed more than fifteen times slower than our "slow" experiment. Under these conditions, the dew point temperature determination could be optimized due to the greater number of measurements made by the weather station. Indeed, averaging over a larger number of measurements made by the station could induce a reduction of the uncertainty on the determination of the dew temperature. In the end, it could lower the uncertainty on the dew formation detection delay especially for the scanning experiment. Also, this slower gradient allows an increased number of points in the moving average on the signal in order to reduce its standard deviation. This could lead to an even more reduced dew detection delay.

Furthermore, the cooled leaf is placed horizontally so that it is cooled as uniformly as possible. Obviously, in the field, the leaves all have a different inclination. As detailed in section III B 3, our measurements show that our method is not very sensitive to this parameter. Hence, this makes us confident in the application of this sensor.

Also, in order to have a first validation of the measurement with the least noise possible, some parameters present in real conditions have been omitted. This includes the presence of wind that will make the leaves oscillate around their equilibrium point as well as the optical path of the beam intercepted by one or more overlapping leaves. Moreover, taking into account parasitic light sources would allow our method to be applicable under different light conditions.

The method detailed here can be compared to other known methods. For example, the method developed by Heusinkveld *et al.* is based on differential spectroscopy using an infrared source[25]. In this case, the measurements can also be made during the day or at night. Moreover, their work highlights the possibility of discriminating the presence of water inside and outside the leaf. However, this discrimination is not always possible. In the current state, our detection is specific to the detection of water on the leaf surface and is not affected by the water inside the leaf. Besides, the work presented by Nikolayev et al.[26] allows to find the surface coverage and the mean radius as long as the drops remain in the size range that still allows efficient diffraction of light. Outside this range, only the surface coverage is recovered. Yet, their approach requires a transparent substrate for the deposited drops and is therefore not suitable for a field application.

The comparison of our experimental results with results from a ray-tracing model has established a good correlation between the experimental signal and the surface coverage. Nevertheless, we have noticed some minor discrepancies between the experimental signal and its modelization. These discrepancies could be reduced using a more sophisticated model. Two ways of improvement can be contemplated. The first one would be to consider a wavelength dependant absorption coefficient for the leaves. The second one would be to describe the leaf itself as a heterogeneous stratified material model, as done by Jacquemoud and Ustin[41].

Additionally, the signal trends of the results presented in Section III A 2 can be reproduced by lowering the contact angle θ_c of each droplet at each time increment. In fact, when the contact angle is lowered faster than the droplet growth, the trend in Fig. 7 or 8a are retrieved. On the contrary, when the droplet growth is faster than the lowering, a trend similar to Fig. 8b is found. In spite of being a well-documented hypothesis[42–44], further work is required to evaluate its validity.

V. CONCLUSION AND OUTLOOKS

In this paper, a new simple method has been proposed to detect water at the surface of leaves, based on the reflection of a laser source in a biaxial configuration. This method partly (for hydrophobic leaves) relies on the Heiligenschein phenomenon, allowing the collection of a significant amount of light returning in direction of the source after being focused by water droplets and reflected by a hydrophobic leaf surface. This light collection is used to assess the average value of all the pixels of the sensor and thus to estimate the leaf wetness status. This method has been successfully applied under controlled conditions on both hydrophobic and hydrophilic surfaces (respectively *Brassica napus* and *Vitis vinifera*) with two distinct cooling rates, for dew formation speed, and with a static or scanning measurement method.

We observed that for both types of surface, the reflected signal is influenced by the presence of water on the leaf surface. However, this influence was opposite depending on whether the surface is hydrophobic or hydrophilic. The signal is respectively increased (up to three times) or decreased (up to half) when dew formation occurs.

When looking specifically at hydrophobic surfaces, the correlation between the received signal and the surface coverage has been established based on 2D ray-tracing numerical simulations. Understandably, the Heiligenschein effect increased the received signal. The dew formation detection delay has been estimated as well as the minimum detectable radius for the dew droplets. When dew evaporated, the signal followed the inverse trend as for dew formation and went back to the normalization value of a dry leaf.

On the hydrophilic surface, as confirmed by ESEM observations, we have observed that the dew droplets readily transformed into more elongated and sophisticated structures, ultimately forming a water film. This water film may act as a scattering optical element. Hence, the more dew on the surface, the lower the signal measured. But, in the case of a slow cooling, a transient Heiligenschein phenomenon can be seen and is then inhibited by droplet coalescence. This hypothesis still needs to be confirmed by simulations. The dew formation detection delay has also been estimated for the hydrophilic surface. During dew evaporation, hydrophilic leaf surface exhibited high signal peaks before going back to the normalization signal.

Similar results were found when using a scanning measurement. This possibly allows mapping wetness at crop scale using laser but experiments on field are needed to confirm this. Initial experiments placed the leaf horizontally to achieve uniform cooling or heating, but this did not accurately reflect the conditions in actual crops. Therefore, a second experiment, focused on how the leaf orientation would impact the signal, was conducted to address this issue. For the hydrophobic surface, the dry surface resulted in an average pixel value diminishing radially around the origin (0°,0°). On the contrary, when the surface was wet, the signal intensity is risen at least by 12.3% and increased again with the angle. For the hydrophilic surface, the average pixel value was 20% lower when the surface was wet than when it was dry. In both cases, the intensity diminished with higher angles. Finally, the maximum gap between dry and wet surfaces is reached when inclination is the highest.

Eventually, when compared to an *in situ* commercial wetness sensor, our device gave, at least, the same amount of information with the added possibility of remote wetness mapping with a single sensor. Detection could be improved by using a more precise dew detection criterion.

Based on the results presented, an in-field application can be considered in the future.

SUPPLEMENTARY INFORMATION

See Supplementary Information for details on the leaf temperature calibration, the similarity between climate chamber and temperature-controlled room measurements, 2D Monte Carlo ray tracing simulations and ESEM observations videos.

AUTHOR CONTRIBUTIONS

All authors contributed to the conceptualization and the methodology of this work. F.G.F. brought the original idea. R.G. set up the experimental hardware, carried out the experiments and analyzed the data. F.G.F and B.M supervised the work and validated the results. R.G and B.M wrote the original manuscript. All authors reviewed the manuscript.

COMPETING INTERESTS

R. Gaetani, F.G. Feugier and B. Masenelli submitted a patent related to this work.

ACKNOWLEDGEMENTS

This work was supported by INSA, INSAVALOR and the Greenshield company. The authors are grateful to Mrs. Elise Lacroix and Franck Bertolla from Université Claude Bernard for careful plant support and use of their climate chambers.

The authors thank Fawzi Karmous (INSA Lyon - Research technician) and Eric Maussière (INSA Lyon - Research technician) for their help in setting up the experiment.

The authors are also grateful to the CLYM (Consortium Lyon Saint-Etienne de Microscopie) and Pr. Karine Masenelli-Varlot (MATEIS) for ESEM observations.

The authors acknowledge support from the Yvan Doyeux (CNRS - IT Engineer) and Newton team from Ecole Centrale de Lyon (Ecully, France), for providing the computing resources needed for this work.

DATA AVAILABILITY STATEMENT

The data that support the findings of this study are available from the corresponding author upon reasonable request.

BIBLIOGRAPHY

[1] Matthew C. Fisher, Daniel. A. Henk, Cheryl J. Briggs, John S. Brownstein, Lawrence C. Madoff, Sarah L. McCraw, and Sarah J. Gurr. Emerging fungal threats to animal, plant and ecosystem health. *Nature*, 484(7393):186–194, 2012.

[2] FAO. *World Food and Agriculture – Statistical Yearbook 2021*. FAO, 2021.

[3] P. K. Gupta, R. R. Mir, A. Mohan, and J. Kumar. Wheat Genomics: Present Status and Future Prospects. *International Journal of Plant Genomics*, pages 1–36, 2008.

[4] Helen Fones and Sarah Gurr. The impact of Septoria tritici Blotch disease on wheat: An EU perspective. *Fungal Genetics and Biology*, 79:3–7, 2015.

[5] A. Calonnec, P. Cartolaro, C. Poupot, D. Dubourdieu, and P. Darriet. Effects of Uncinula necator on the yield and quality of grapes (Vitis vinifera) and wine. *Plant Pathology*, 53(4):434–445, 2004.

[6] E.S. Scott, R.G. Dambergs, and B.E. Stummer. Fungal contaminants in the vineyard and wine quality. In *Managing Wine Quality*, pages 481–514. Elsevier, 2010.

[7] NV Hardwick, Bruce DL Fitt, Stuart J Wale, JB Sweet, et al. Oilseed rape diseases. *Oilseed rape diseases.*, 1(OS4), 1991.

[8] HA McCartney, KJ Doughty, G Norton, EJ Booth, SPJ Kightley, G Landon, G West, KC Walker, and JE Thomas. A study of the effect of disease on seed quality parameters of oilseed rape. *Proc 10th Intern Rap Cong, Canberra, Australia*, 1999.

[9] Bronislava Butkutė, Gvidas Šidlauskas, and Irena Brazauskienė. Seed Yield and Quality of Winter Oilseed Rape as Affected by Nitrogen Rates, Sowing Time, and Fungicide Application. *Communications in Soil Science and Plant Analysis*, 37(15-20):2725–2744, 2006.

[10] Fausto Almeida, Marcio L. Rodrigues, and Carolina Coelho. The Still Underestimated Problem of Fungal Diseases Worldwide. *Frontiers in Microbiology*, 10:214, 2019.

[11] Michael C.R. Alavanja, Jane A. Hoppin, and Freya Kamel. Health Effects of Chronic Pesticide Exposure: Cancer and Neurotoxicity. *Annual Review of Public Health*, 25(1):155–197, 2004.

[12] Dorothée Provost, Anne Cantagrel, Pierre Lebailly, Anne Jaffré, Véronique Loyant, Hugues Loiseau, Anne Vital, Patrick Brochard, and Isabelle Baldi. Brain tumours and exposure to pesticides: A case–control study in southwestern France. *Occupational and Environmental Medicine*, 64(8):509–514, 2007.

[13] Ming Ye, Jeremy Beach, Jonathan W. Martin, and Ambikaipakan Senthilselvan. Pesticide exposures and respiratory health in general populations. *Journal of Environmental Sciences*, 51:361–370, 2017.

[14] Daniela Laurino, Aulo Manino, Augusto Patetta, and Marco Porporato. Toxicity of neonicotinoid insecticides on different honey bee genotypes. *Bulletin of Insectology*, 66(1):8, 2013.

[15] Muyesaier Tudi, Huada Daniel Ruan, Li Wang, Jia Lyu, Ross Sadler, Des Connell, Cordia Chu, and Dung Tri Phung. Agriculture Development, Pesticide Application and Its Impact on the Environment. *International Journal of Environmental Research and Public Health*, 18(3):1112, 2021.

[16] Hideo Ishii and Derek William Hollomon, editors. *Fungicide Resistance in Plant Pathogens*. Springer Japan, 2015.

[17] Jason R. Rohr, Jenise Brown, William A. Battaglin, Taegan A. McMahon, and Rick A. Relyea. A pesticide paradox: Fungicides indirectly increase fungal infections. *Ecological Applications*, 27(8):2290–2302, 2017.

[18] Department of Computer Technology, Yeshwantrao Chavan College of Engineering, Nagpur, Maharashtra, India., Ms. Kiran R. Gavhale, and Prof. Ujwalla Gawande. An Overview of the Research on Plant Leaves Disease detection using Image Processing Techniques. *IOSR Journal of Computer Engineering*, 16(1):10–16, 2014.

[19] S Arivazhagan, R Newlin Shebiah, S Ananthi, and S Vishnu Varthini. Detection of unhealthy region of plant leaves and classification of plant leaf diseases using texture features. *Agricultural Engineering International: CIGR Journal*, 15:7, 2013.

[20] T. Rumpf, A.-K. Mahlein, U. Steiner, E.-C. Oerke, H.-W. Dehne, and L. Plümer. Early detection and classification of plant diseases with Support Vector Machines based on hyperspectral reflectance. *Computers and Electronics in Agriculture*, 74(1):91–99, 2010.

[21] Virginie Lacotte, Sergio Peignier, Marc Raynal, Isabelle Demeaux, François Delmotte, and Pedro da Silva. Spatial–Spectral Analysis of Hyperspectral Images Reveals Early Detection of Downy Mildew on Grapevine Leaves. *International Journal of Molecular Sciences*, 23(17):10012, 2022.

[22] Gemma Hornero, Jorge E. Gaitán-Pitre, Ernesto Serrano-Finetti, Oscar Casas, and Ramon Pallas-Areny. A novel low-cost smart leaf wetness sensor. *Computers and Electronics in Agriculture*, 143:286–292, 2017.

[23] Kamlesh S. Patle, Biswajit Dehingia, Hemen Kalita, and Vinay S. Palaparthy. Highly sensitive graphene oxide leaf wetness sensor for disease supervision on medicinal plants. *Computers and Electronics in Agriculture*, 200:107225, 2022.

[24] Lei Zhu, Zhiguo Cao, Wen Zhuo, Ruicheng Yan, and Shuqing Ma. A New Dew and Frost Detection Sensor Based on Computer Vision. *Journal of Atmospheric and Oceanic Technology*, 31(12):2692–2712, 2014.

[25] B.G. Heusinkveld, S.M. Berkowicz, A.F.G. Jacobs, W. Hillen, and A.A.M. Holtslag. A new remote optical wetness sensor and its applications. *Agricultural and Forest Meteorology*, 148(4):580–591, 2008.

[26] Vadim S. Nikolayev, Patrick Sibille, and Daniel A. Beysens. Coherent light transmission by a dew pattern. *Optics Communications*, 150(1-6):263–269, 1998.

[27] Richard M. Schotland, Kenneth Sassen, and Richard Stone. Observations by Lidar of Linear Depolarization Ratios for Hydrometeors. *Journal of Applied Meteorology*, 10(5):1011–1017, 1971.

[28] Łukasz Lasyk, Michał Łukomski, and Lukasz Bratasz. Simple digital speckle pattern interferometer (DSPI) for investigation of art objects. *Optica Applicata*, 41, 2011.

[29] Mohammad R. Riahi, Hamid Latifi, and Mohsen Sajjadi. Speckle correlation photography for the study of water content and sap flow in plant leaves. *Appl. Opt.*, 45(29):7674–7678, 2006.

[30] Jan O. Mattsson and Christian Cavallin. Retroreflection of Light from Drop-Covered Surfaces and an Image-Producing Device for Registration of This Light. *Oikos*, 23(3):285, 1972.

[31] Yong He, Shupei Xiao, Jianjian Wu, and Hui Fang. Influence of Multiple Factors on the Wettability and Surface Free Energy of Leaf Surface. *Applied Sciences*, 9(3):593, February 2019.

[32] Christoph Konlechner and Ursula Sauer. Ultrastructural leave features of grapevine cultivars (vitis vinifera l. ssp. vinifera). *OENO One*, 50(4), 2016.

[33] D Beysens. *Dew Water*. River Publishers, 2018.

[34] Craig F. Bohren and Donald R. Huffman. *Absorption and scattering of light by small particles*. Wiley-VCH, 2004.

[35] Jan O. Mattsson and Lars Bärring. Heiligenschein and related phenomena in divergent light. *Applied Optics*, 40(27):4799, 2001.

[36] A. Leigh, S. Sevanto, J.D. Close, and A.B. Nicotra. The influence of leaf size and shape on leaf thermal dynamics: Does theory hold up under natural conditions? *Plant, Cell & Environment*, 40(2):237–248, 2017.

[37] William W. Cure, Richard B. Flagler, and Allen S. Heagle. Correlations between canopy reflectance and leaf temperature in irrigated and droughted soybeans. *Remote Sensing of Environment*, 29(3):273–280, 1989.

[38] Viridiana Silva-Perez, Gemma Molero, Shawn P Serbin, Anthony G Condon, Matthew P Reynolds, Robert T Furbank, and John R Evans. Hyperspectral reflectance as a tool to measure biochemical and physiological traits in wheat. *Journal of Experimental Botany*, 69(3):483–496, 2018.

[39] Why painting and calibrating your leaf wetness sensor won't work, 2021. `https://www.metergroup.com/en/meter-environment/measurement-insights/why-painting-and-calibrating-your-leaf-wetness-sensor`.

[40] Prevision-meteo.ch. Relevés horaires des observations météo de lyon / bron pour la journée du lundi 01 août 2022, 2022. `https://prevision-meteo.ch/climat/horaire/lyon-bron/2022-08-01`.

[41] Stéphane Jacquemoud and Susan Ustin. *Leaf Optical Properties*. Cambridge University Press, 1 edition, 2019.

[42] S. Vafaei and M.Z. Podowski. Analysis of the relationship between liquid droplet size and contact angle. *Advances in Colloid and Interface Science*, 113(2-3):133–146, 2005.

[43] Jimin Park, Hyung-Seop Han, Yu-Chan Kim, Jae-Pyeong Ahn, Myoung-Ryul Ok, Kyung Eun Lee, Jee-Wook Lee, Pil-Ryung Cha, Hyun-Kwang Seok, and Hojeong Jeon. Direct and accurate measurement of size dependent wetting behaviors for sessile water droplets. *Scientific Reports*, 5(1):18150, 2015.

[44] S.Y. Misyura. Contact angle and droplet evaporation on the smooth and structured wall surface in a wide range of droplet diameters. *Applied Thermal Engineering*, 113:472–480, 2017.